The Observation of High-Order Charge–Current Configurations in Plasmonic Meta-Atoms: A Numerical Approach

Burak Gerislioglu and Arash Ahmadivand *

Department of Physics and Astronomy, Rice University, 6100 Main St, Houston, TX 77005, USA; bg29@rice.edu
* Correspondence: aahmadiv@rice.edu

Abstract: Living in a world of resonances, there have been significant progresses in the field of excitation of pronounced and multifunctional moments across a wide range of optical frequencies. Among all acknowledged resonances, the toroidal multipoles have received copious interest in recent years due to possessing inherent signatures in nature. As a fundamental member, toroidal dipole is a strongly localized electromagnetic excitation based on charge–current configurations, which can be squeezed into an extremely small spot. Although there have been extensive studies on the behavior and properties of toroidal dipoles in order to develop all-optical devices based on this technology, so far, all analyses are restricted to the first (1st) order toroidal dipoles. In this work, using a practical technique, we successfully observed exquisite multi-loop super-toroidal (MLST) spectral features in a planar multipixel metallodielectric meta-atom. Employing the theory behind the excitation of multi-loop currents, we numerically and theoretically demonstrated that a traditional toroidal dipole can be transformed into a super-toroidal moment by varying the dielectric permittivity of the capacitive gaps between proximal pixels. This understanding introduces a new approach for the excitation of complex multi-loop toroidal moments in plasmonic metamaterials with high sensitivity, applicable for various nanophotonics applications from sensing to filtering.

Keywords: toroidal dipole; plasmonic meta-atoms; multi-loop currents; super-toroidal moment

1. Introduction

Charge–current configurations in the static form possess a perceivable signature at both the nucleic and giant (galaxies, neutron starts, black holes, and quasars) levels, where the electromagnetic properties of these multipole excitations, arising from any complex system in particular, have been described quantitatively by multipole expansions in electrodynamics principles [1–3]. Such unconventional charge–current excitations (i.e., ring currents, poloidal magnetic fields, toroidal modes, flying doughnuts, and anapole states) with dramatically concealed far-field radiation patterns have been classified in a different family of multipoles [4]. In the subwavelength optical systems limit, the loop-currents have successfully been induced either in artificial 3D or planar all-dielectric and plasmonic metamolecules [4,5]. Enforcing simultaneous time-reversal ($t{\rightarrow}-t$) and space-inversion ($r{\rightarrow}-r$) violations and applying light to the subwavelength systems enables the excitation of significantly squeezed, gyrotropic-fashioned rotating magnetic fields, known as "dynamic toroidal multipoles" [4,6]. Because of dramatic masking by dominant classical electromagnetic far-field radiations, toroidal topology provides a nonzero contribution to the emitted radiation from a scatterer. Among toroidal multipoles, of particular interest is the dynamic toroidal dipole, the fundamental member of toroidal multipoles, which has been analysed in metamaterials and utilized extensively for developing advanced technologies and practical devices from immunosensors to modulators [5,7–11]. Such extensive interests

originate from the inherent nonradiative property of toroidal dipoles due to suppression of the radiative electric dipolar mode. In terms of the toroidization principle, this mode forms due to the combination of a magnetic quadrupole and an electric octupole, in which the optically driven dynamic toroidal dipole can be imagined as magnetically induced currents fluxing across the surface of a torus, also known as poloidal currents or loop currents [4,5,12–14].

Artificially engineered all-dielectric and metallic metamaterials are promising subwavelength platforms to excite pronounced and narrow toroidal resonances [15–17]. Traditionally, metasurfaces mimic the visual torus arrangement for the electromagnetic excitation of the toroidal dipole spectral feature. Besides numerical and theoretical studies, recently Xu et al. [18] experimentally perceived the excitation of toroidal dipoles in all-dielectric metamaterials. In spite of such a vast research on the physics and applications of toroidal dipole moments, the orders of the toroidal currents that have been reported are limited to "zero" and "one", while the excitation of toroidal modes with multiple loop-currents, or super-toroidal currents, has never been observed in typical metamaterial platforms. Toroidal currents with different orders (>1) can be visualized as twisted doughnut-shape configurations. Depending on the number of these loop-currents, the super-toroidal current configurations can be simply categorized in odd and even-orders. As promising tools, numerical techniques help us to understand the possibility of the formation of multi-loop super-toroidal (MLST) current arrangements in plasmonic metasurfaces.

In this report, we develop an asymmetric meta-atom to address this fundamental shortcoming in the toroidal moment's theory. Here, we report on the first numerical observation of the excitation of MLST modes in planar metallodielectric metamaterials, verified by applying the theoretical physics behind it. To this end, we tailor a multicomponent unit cell consisting of aluminum (Al) nanopixels and alumina (Al_2O_3) spacers to induce high order charge–current configurations across the near-infrared (NIR) band. To excite the super-toroidal spectral feature, we enhanced the plasmon coupling effect between the proximal nanopixels resonators via introducing alumina spacers at the specific capacitive gaps. Our findings show how the multi-loop modes can be excited and observed in nanoplasmonic meta-atoms.

2. The Theory of High-Order Toroidal Solenoids

In this section, we firstly summarize the utilized theory of the excitation of high-order toroidal solenoids to validate the simulation studies. By considering a circular current loop located in the $z = 0$ plane with its symmetry along the z-axis (for the 0th order mode plotted in Figure 1A), the induced current is given by [19,20]:

$$\vec{J} = \vec{n}_\varphi I \delta(\rho - d)\delta(z) \tag{1}$$

where d is radius of the loop and $\vec{n}_\varphi$ is unit vector tangent to the plane of the loop. Since $\nabla \cdot \vec{J} = 0$, the current flowing for the 0th mode can be depicted by an analogous magnetization concept ($\vec{M}$):

$$\vec{M} = \vec{n}_z I \zeta(d - \rho)\delta(z), \text{ as } \vec{J} = \nabla \times \vec{M} \tag{2}$$

where $\zeta(\square)$ is a step function. This equation can also be interpreted as an expression of Ampere theorem, in which the closed circular current is equivalent to the magnetic moment normal to it [21]. It should be underlined that the induced magnetic field can be derived from Equations (1) and (2), and the related magnetic vector potential can be written as:

$$\vec{B} = \frac{I}{c}\int \frac{1}{\left|\vec{r} - \vec{r}'\right|} \vec{n}_{\varphi'}\delta(\rho' - d)\delta(z')dV' \tag{3}$$

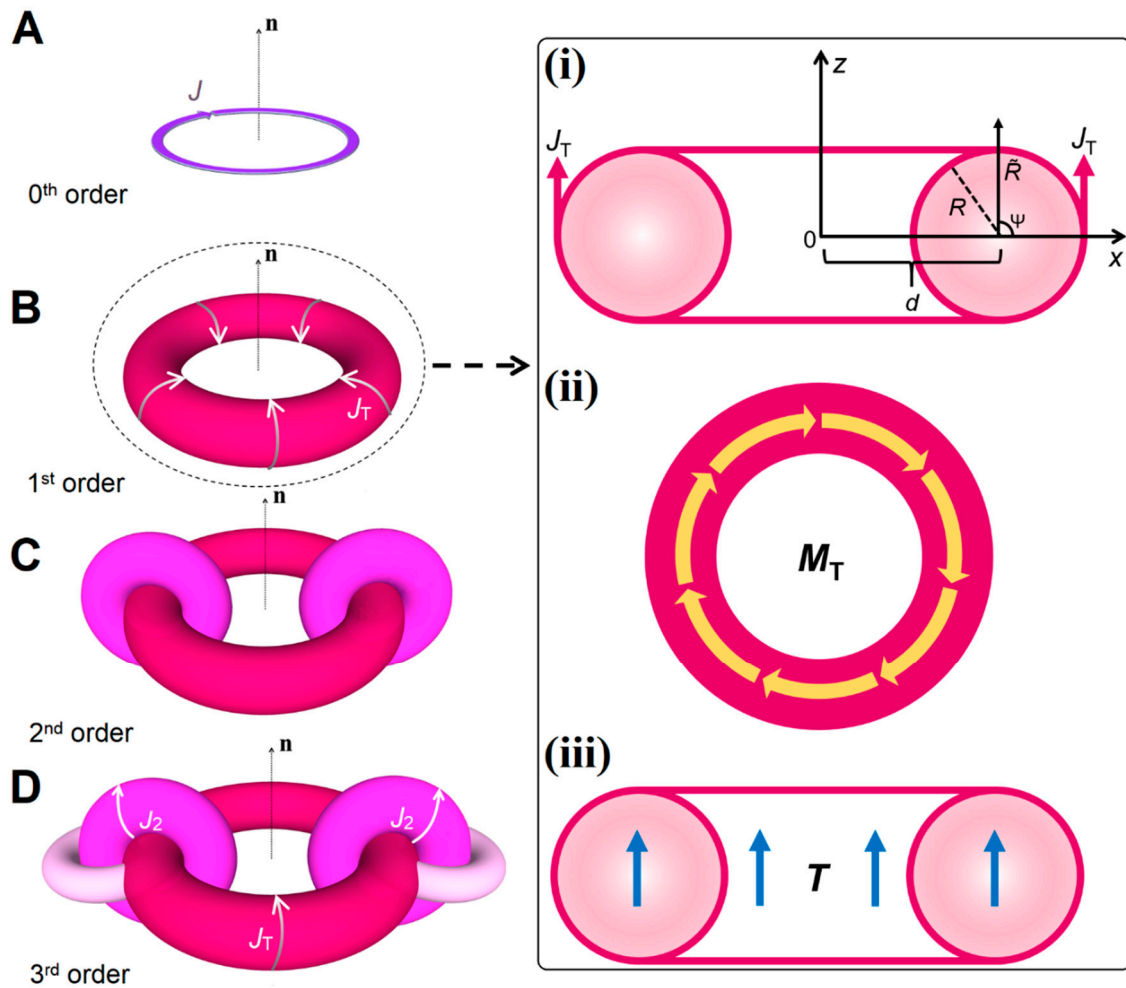**Figure 1.** (**A**) Current distribution representation of a circular current-loop for a magnetic dipole. (**B**) Current-carrying, firmly winded (where the helicity of the solenoid vanishes) toroidal solenoid of 1st order. It can also be considered as a source of a toroidal dipole. The arrows demonstrate the poloidal currents flowing on the surface of an imaginary torus (i). Here, the torus is intensively wrapped by the magnetized rings (ii). The directed toroidization along the axis of the torus (iii). (**C**) Current-carrying, tightly winded toroidal solenoid of 2nd order (super-toroidal wire coil, pink-colored). The arrows indicate the related poloidal currents of the 2nd order toroidal solenoid, flowing on the surface of the pink-colored torus. (**D**) Current-carrying, closely winded toroidal solenoid of 3rd order (super-toroidal wire coil, pale pink-colored). The arrows indicate the corresponding poloidal currents of the 3rd order toroidal solenoid, flowing on the surface of the pale pink-colored torus.

For very small radiuses (d), $\vec{J}$ is not well-described because the unit vector tangent is no longer valid at the origin, while $\vec{M}$ is still well-expressed. Furthermore, when d tends to zero ($d \to 0$) in Equation (1), we will have a magnetic dipole moment as a result of very small values of d.

When we take into account a more complicated system (as indicated in Figure 1B for the 1st order mode), a poloidal current flows on the surface of the magenta-colored torus along its meridians, which can be formulated as:

$$\vec{J}_T = -\frac{\Phi c \delta(R - \widetilde{R}) \vec{n}_\psi}{8\pi^2 (d - \sqrt{d^2 - R^2})(d + \widetilde{R} \cos \psi)} \tag{4}$$

where $\vec{n}_\psi$ is the unit vector tangent to the magenta-colored torus surface ($\vec{n}_\psi = \vec{n}_z \cos \psi - \vec{n}_\rho \sin \psi$) and Φ is the magnetic flux which penetrates to the torus. For Equation (4), the following is assumed: $\widetilde{R}, \psi$, and ϕ are the corresponding Cartesian coordinates:

$$x = (d + \widetilde{R}\cos\psi)\cos\phi$$
$$y = (d + \widetilde{R}\cos\psi)\sin\phi \tag{5}$$
$$z = \widetilde{R}\sin\psi$$

Furthermore, the surface of the magenta-colored torus can be envisioned where $R = \widetilde{R}$. By manipulating the ψ, ϕ, and for a fixed $\widetilde{R}$, one can claim that the x, y, and z points mentioned above can fill the surface where $(\rho - d)^2 + z^2 = R^2$ (see Figure 1B(i)). Similar to the 0th mode case, for $\nabla \cdot \vec{J}_T = 0$, $\vec{J}_T$ (see Figure 1B) can be written in terms of magnetization ($\vec{M}_T$) (see Figure 1B(ii)), in which $\vec{M}_T$ is confined within the magenta-colored torus, and has only ϕ component (which only varies inside the torus) as following [21]:

$$\vec{M}_T = \frac{\Phi c \vec{n}_\phi}{8\pi^2 \rho (d - \sqrt{d^2 - R^2})} \zeta(R - \sqrt{(\rho - d)^2 + z^2}) \tag{6}$$

Since $\nabla \cdot \vec{M} = 0$, the resulting toroidization ($\vec{T}$) (see Figure 1B(iii)) is: $\vec{M} = \nabla \times \vec{T}$, where $\nabla \cdot \vec{T} \neq 0$. In light of the toroidization and Equation (6), the poloidal current in Equation (4) is equal (in terms of inducing same magnetic field) to the magnetization and to the toroidization, which are the extensions of Ampere's law. Additionally, one can deduce the following as toroidization:

$$\frac{\vec{T}}{\vec{n}_z} = \frac{c\Phi}{8\pi^2(d - \sqrt{d^2 - R^2})} \left(\zeta(d - \sqrt{R^2 - z^2} - \rho) \ln \frac{d + \sqrt{R^2 - z^2}}{d - \sqrt{R^2 - z^2}} \right.$$
$$\left. + \zeta(d + \sqrt{R^2 - z^2} - \rho)\zeta(\rho - d + \sqrt{R^2 - z^2}) \times \ln \frac{d + \sqrt{R^2 - z^2}}{\rho} \right) \tag{7}$$

Furthermore, based on different regions in space, $\frac{\vec{T}}{\vec{n}_z}$ has different expressions:

$$\begin{cases} \frac{\vec{T}}{\vec{n}_z} = \frac{c\Phi}{8\pi^2(d - \sqrt{d^2 - R^2})} \ln \frac{d + \sqrt{R^2 - z^2}}{d - \sqrt{R^2 - z^2}}, \text{ where } 0 \leq \rho \leq (d - \sqrt{R^2 - z^2}) \\ \frac{\vec{T}}{\vec{n}_z} = \frac{c\Phi}{8\pi^2(d - \sqrt{d^2 - R^2})} \ln \frac{d + \sqrt{R^2 - z^2}}{\rho}, \text{ where } (d - \sqrt{R^2 - z^2}) \leq \rho \leq (d + \sqrt{R^2 - z^2}) \end{cases} \tag{8}$$

In other domains, $\frac{\vec{T}}{\vec{n}_z}$ will be zero. Based on Equations (7) and (8), one can say that extracting the $\vec{T}$ seems complicated. To overcome this, a volume integral can be applied:

$$\int \vec{T} dV = \frac{c\pi R^2 d\Phi \vec{n}_z}{8\pi(d - \sqrt{d^2 - R^2})} \tag{9}$$

So far, we explained the theory behind the formation of zero and first order loop currents based on the toroidization principle. Using a similar approach to continue, we focus on the possibility and theory of the excitation of the second and third order of loop currents. Indeed, the study of each possible multipole correlating with a given multipole decomposition scheme (i.e., for electric, magnetic, or toroidal modes) is quite challenging in terms of toroidal multimodes, which have traditionally failed to be noticed. Nevertheless, they have a key role in the field of nanophotonics and plasmonics [4]. As indicated by Nemkov et al. [22], the decomposition scheme generates high-order modes within the hierarchy of a toroidal system (i.e., toroidal solenoid), known as "mean-square radii" of the induced toroidal mode. It is noteworthy to mention that without complementing the multipole expansion with these high-order terms, the decomposition will be incorrect [23]. Hence, under illumination with an incident light, each term in a dynamic mode decomposition supports only a specific angular projection

of the charge–current distribution. Moreover, in the context of mean-square radii, one can easily explore its 1st order of an electric or a magnetic dipole, as demonstrated previously in Nemkov et al. [22]. By centering on the super-toroidal modes from the quantitative perspective, we first study the hierarchy of a toroidal solenoid system, in which each turn of it can be considered as another toroidal solenoid. For simplicity, the elucidation of the super-toroidal moments will be established on a simple current loop approximation. In this regard, when the radius of the magenta-colored torus (R) in Figure 1B tends to zero (i.e., infinitely thin toroidal solenoid), the following can be concluded [21]:

$$\frac{\vec{T}}{\vec{n}_z} = \frac{c\Phi}{4d\pi^2(d - \sqrt{d^2 - R^2})}\zeta(d - \rho)\sqrt{R^2 - z^2} \tag{10}$$

where the second term of Equation (7) is shortened to Equation (10). For an infinitesimally small R, $\sqrt{R^2 - z^2}$ can be written as $R^2\pi\delta(z)/2$. Thus, the poloidal current tends to $\nabla \times (\nabla \times \vec{T})$, where $\vec{T} = \frac{\vec{n}_z R^2 \Phi c}{8d\pi(d - \sqrt{d^2 - R^2})}\delta(z)\zeta(d - \rho)$, and one can mention that $\vec{T}$ is constricted within the interior of the current-carrying coil and is perpendicular to it. In addition to $R \to 0$, when we consider $d \to 0$, the right hand side of the previous equation will be $\vec{n}_z \frac{\Phi c R^2 d}{16\rho\pi(d - \sqrt{d^2 - R^2})}\delta(z)\delta(\rho)$.

Furthermore, we envision the following high-order feature (2nd order) as our first super-toroidal mode of the proposed system, in which the related moment is indicated as a tightly winded, pink-colored toroidal wire coil in Figure 1C. As each turn of a series of toroidal solenoids is again an individual toroidal solenoid, we can easily set up a new toroidal wire coil onto each of the former ones. In this fashion, the next mode (3rd order) will be our second super-toroidal feature of the given platform, where it is displayed as a firmly winded, pale pink-colored torus in Figure 1D. For convenience, only certain regions of the induced super-toroidal modes are shown. Furthermore, the second phase of the toroidal source can be observed from the first super-toroidal mode, where $\vec{J}_2$ moves in its windings. Based on the previously explained magnetization concept, one can state that the $\vec{J}_2$ induces the corresponded $\vec{M}_2$ (super-positioned magnetizations from each winding) on the surface of the initial toroidal solenoid (see Figure 1D) along its meridians, and the resulting $\vec{M}_2$ will generate the first, closed-chain super-toroidal moment. Consequently, the following relation can be written:

$$\vec{J}_2 = \nabla \times (\nabla \times (\nabla \times \vec{T}_2)) \text{ or } \vec{J}_2 = \left(\frac{\Phi c R^2 d}{16\rho\pi(d - \sqrt{d^2 - R^2})}\delta(z)\delta(\rho)\right)\nabla \times (\nabla \times (\nabla \times \vec{n}\delta^{(3)}(\vec{r}))) \tag{11}$$

For an arbitrary super-toroidal mode (i), $\vec{J}_i = \left(\frac{\Phi c R d}{8\rho\pi(d - \sqrt{d^2 - R^2})}\delta(z)\delta(\rho)\right)\nabla^{(i+1)} \times (\vec{n}\delta^{(3)}(\vec{r}))$ is valid, where $\vec{r}$ is used to generalize the formula. By following a similar method as was applied for the first super-toroidal moment, one can subsequently easily describe the second super-toroidal mode of the proposed system.

3. Results

In Figure 2A, we artistically demonstrated the formation of multi-loop currents in the proposed nanostructure, which is imagined based on our numerical observations. This illustration gives a brief overview for the professed assertion and formation of an MLST mode. The corresponding geometrical sizes for the structure are exhibited in Figure 2B, as top-view images for the vacuum condition and the presence of alumina spacers in the openings between adjacent resonators, distinguished by a different color. Under y-polarized (TE) beam illumination, one can see the excitation of pronounced toroidal dipole modes around $\lambda \sim 1$ μm and $\lambda \sim 1.1$ μm for the gaps in vacuum and alumina-filled regimes, respectively (Figure 2C). The transmission (Γ) spectra reveals the formation of two minima across the NIR band, corresponding to double directional toroidal dipoles, driven by the poloidal fields and loop-currents [12]. Here, we merely consider the targeted mode at shorter wavelengths for the

excitation of a super-toroidal feature. The distinct red-shift (around $\delta\lambda \sim 100$ nm) in the position of toroidal dipole originates from the dielectric permittivity variations in the capacitive spots. In addition, to show how correct the theoretical analyses are, we computed and compared the transmission spectra in Figure S1 (Supporting Information). This panel confirms perfect consistency between the accurate numerical analysis and the used theory in *Kong* [24]. The characteristic electric and magnetic-field (E- and H-field) maps allow one to understand the excitation of the toroidal feature. The 3D |E|-field map in Figure 2D illustrates strong E-field confinement at the capacitive gaps (with alumina spacers), nonetheless, the intensity of the field enhancement at the opening areas close to the center of the unit cell is much stronger. This is due to the formation of an oblique toroidal mode spinning across the peripheral curved pixels, arising due to the magnetic field mismatch at these resonators. The |H|-field snapshot (in Figure 2E) confirms the realization of an oblique moment and strong confinement of magnetic fields across the curved resonators. The strong H-field confinement is demonstrated in the cross-sectional plane (*z*-axis) as a function of incident beam wavelength in Figure 2F. The results in this snapshot are consistent with the cross-sectional H-field confinement within the nanostructure, as shown in Figure S2 (Supporting Information). If excited at resonance, the contribution of the magnetic field to the scattered radiation from the scatterer (around $\lambda \sim 1.1$ μm) is much stronger. Although the excitation of the oblique toroidal dipole in the proposed meta-atom is a unique feature, there is a hidden phenomenon in the structure, which will be explained in the following part. In Figure 3A, the excitation of a toroidal dipole in a vacuum condition is proved by showing the strength of multipole excitations for the power of the scattered multipoles emitting from the meta-atom. In this mode analysis graph, the main contributors to the unit cell spectral response are the electric dipole (**p**), in conjunction with a superposition of well-matched toroidal dipolar (**T**), and magnetic quadrupolar ($\mathbf{Q^{(m)}}$) moments. We also depicted the verification of the electromagnetic multipoles up to the 3rd order toroidal solenoid to deliver explicit information about their impact on the current configurations in the proposed platform in Figure 3B,C. To this end, we checked the (i) electric 16-pole and magnetic octupole (which are the basis of the 2nd order toroidal solenoid) and the (ii) electric 32-pole and magnetic 16-pole (which are the foundation of the 3rd order toroidal solenoid).

Figure 1A shows that the toroidal currents hierarchy is employed to define the theory and notations in the following descriptions. This profile contains the toroidal dipole from the 0th order to the 3rd order. Figure 4A,B compare the formation of the toroidal dipole moments in a vacuum and the presence of an alumina capacitive spacer, respectively, at and around the resonance wavelengths as vectorial H-field maps in *xz*-planes. Here, we try to monitor the quality of the toroidal spectral feature in the vicinity of the central wavelength to be sure about our claim. Clearly, for the vacuum condition, the toroidal moment is robust at $\lambda \sim 1$ μm, and keeps its nature around the resonance position (± 50 nm) and vanishes at further wavelengths. The noteworthy point here is the formation of a single toroidal loop-current at all wavelengths, corresponding with the 1st order toroidal current. On the other hand, for the presence of an alumina spacer at the gaps, we observed a distinguished toroidal loop-current at $\lambda \sim 1.1$ μm. In this regime, the peripheral vectorial loops are correlated with the third loop-current (J_3), keeping their strength around the original feature at 100 nm away from the resonance wavelength. It should be underlined that due to representing the vectorial boards in 2D panels, it is challenging to plot all loops simultaneously. To investigate the possibility of the generation of the third toroidal current loops, one should monitor the other planes (*xy* and *yz*-planes) around the unit cell to monitor the presence of (J_2). Figure 4C,D illustrate and evaluate the vectorial maps in the *yz*-plane for the excitation of a second loop-current (J_2) in the vacuum and alumina-filled gap regimes, respectively. Clearly, for the gaps without the spacer, the projected magnetic field is not perturbed, while for gaps with an alumina spacer, a spinning pattern is formed correlating with the second loop (J_2). This strongly verifies the excitation of the super-toroidal spectral feature in the proposed plasmonic meta-atom.
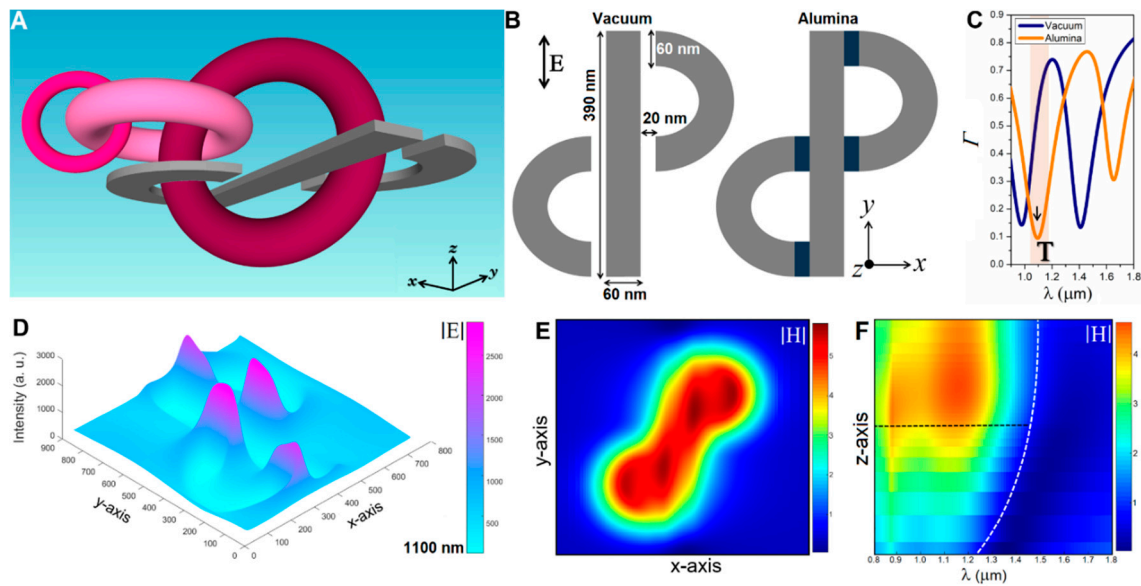
Figure 2. (**A**) An artistic rendering of the proposed toroidal plasmonic meta-atom, holding multiple twisted loop-currents. (**B**) Top-view images of the unit cell for the absence and presence of an alumina spacer at the gaps with a description of the geometrical sizes. (**C**) Transmission (Γ) amplitude for the excitation of the toroidal feature under polarized normal beam excitation for two different analyzed regimes. (**D**) The 3D |E|-field map for the excitation of the toroidal feature in the presence of an alumina spacer at the resonance wavelength ($\lambda \sim 1100$ nm). (**E**) The 2D |H|-field map for the excitation and localization of the magnetic field, leading to inducing an oblique toroidal feature at 1100 nm. (**F**) The cross-sectional |H|-field snapshot as a function of the incident beam, validating emission of a huge field from the toroidal scatterer at the resonance wavelength.
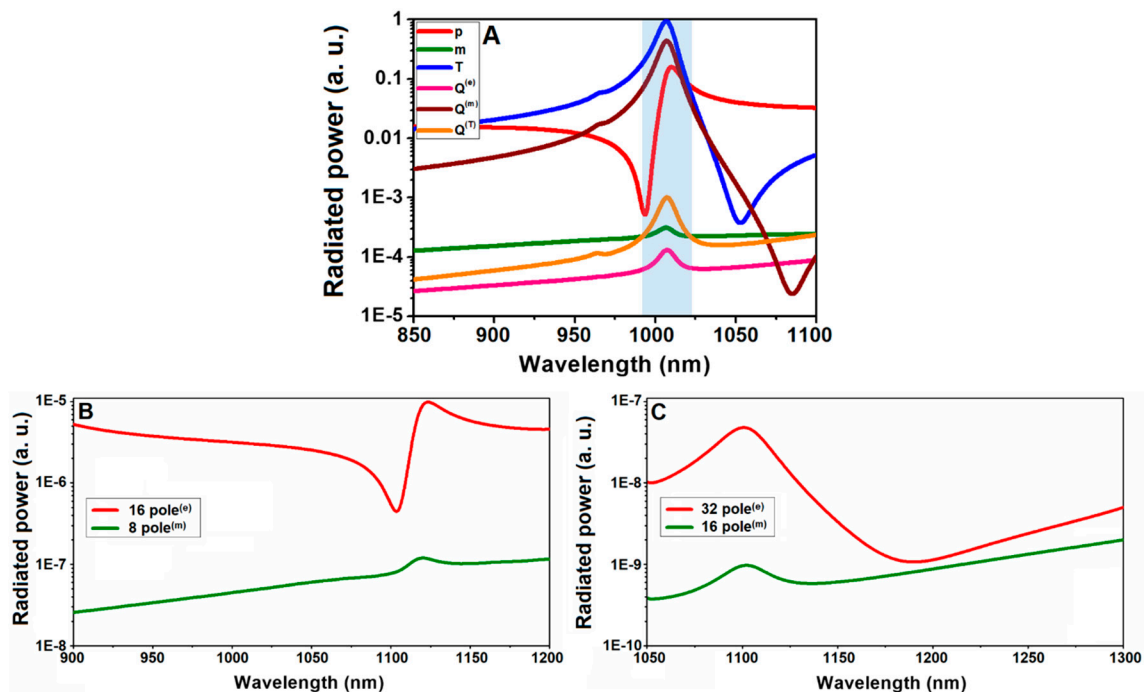

Figure 3. Calculated radiated power of individual electromagnetic multipoles excited in the meta-atom for (**A**) the 1st order toroidal solenoid and high-order toroidal moments: (**B**) the 2nd order toroidal solenoid and (**C**) the 3rd order toroidal solenoid.
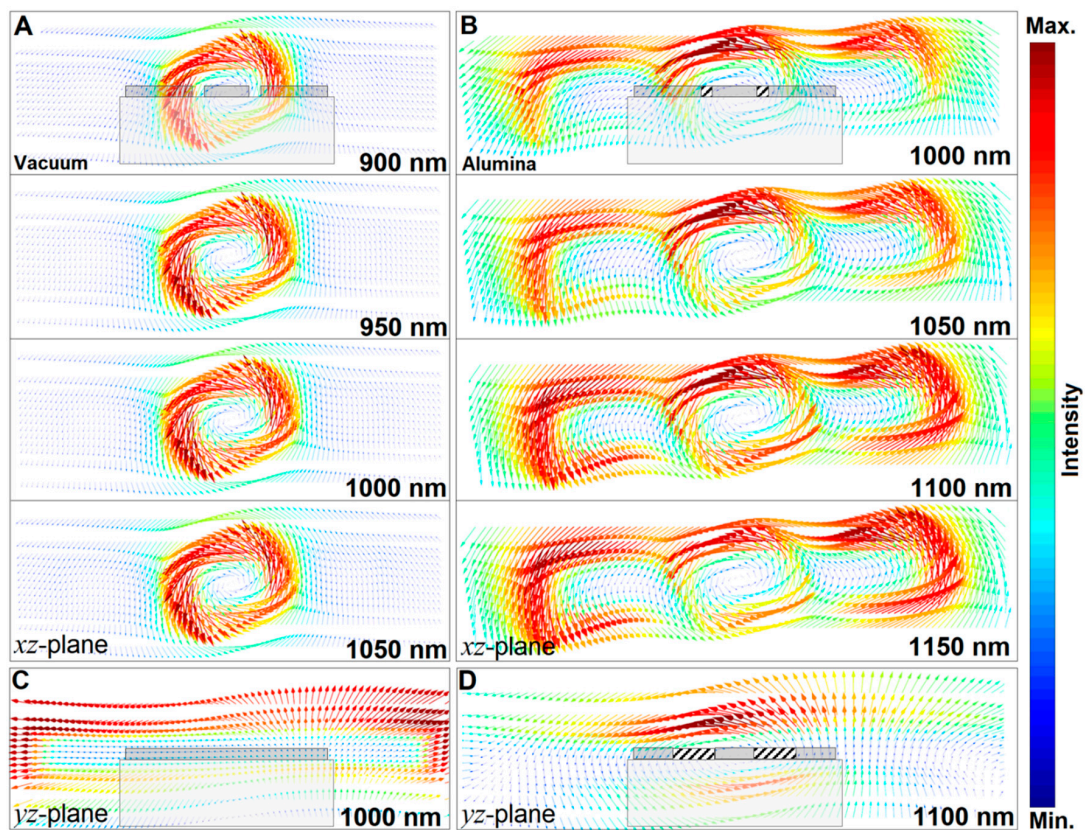
Figure 4. (**A**,**B**) Vectorial H-field panels for the formation of the 1st order toroidal and super-toroidal features in the *xz*-planes, respectively. In (**B**) the appeared peripheral loops around the central feature correspond with the first order super toroid. (**C**,**D**) Vectorial H-field maps in the *yz*-planes for the possibility of the excitation of the second order super toroid, in vacuum and alumina-filled gap regimes, respectively, showing the absence of the current-loop in the vacuum spacer and formation of the additional loop in the presence of the alumina piece.

To explore the influence of the variations in the gaps' permittivity, one should examine the relation between toroidal currents and dielectric variations [25,26]. To underlay the physics behind the formation of the MLST signature, one needs to investigate the influence of the capacitive spacer on the spectral response of the metasurface as a key parameter. Given that the projected toroidal dipole currents strongly depend on the surrounding complex dielectric permittivity ($T = -J_T L c^2 / \omega^2 \widetilde{\varepsilon}$ and $T_i = -J_i c^2 / \omega^2 \widetilde{\varepsilon}$ ($i = 2, 3 \ldots$)), in which L is the length of the dipole, therefore, controlling the excitation of multiple toroidal components and loops could be possible by applying variations in the dielectric permittivity at the critical areas of the structure and vice versa. In other words, varying the ratio between the amplitudes of the currents flowing in the toroidal dipole can be accomplished by tuning the complex dielectric of the medium. As the gaps play a fundamental role in the plasmonic response of the proposed unit cell, subtle perturbations in the dielectric permittivity of gaps alter the spectral behavior of the entire metasurface.

Ultimately, we analyzed the induced current density due to the formation of a multi-loop spectral feature, as shown in Figure 5. This spectral image (*xz*-axis) allows one to compare the induced current density in the presence and absence of an alumina capacitive spacer at the gap regions. Obviously, in the vacuum limit, a dominant extreme associating with the toroidal dipole feature arises, while for the presence of alumina in the gaps, a second peak is induced corresponding to the additional loop-currents, having an amplitude analogous to the original peak. It should be noted that a small shoulder in the current map in the vacuum regime is formed due to the poloidal current of the 1st order toroidal dipole moment.
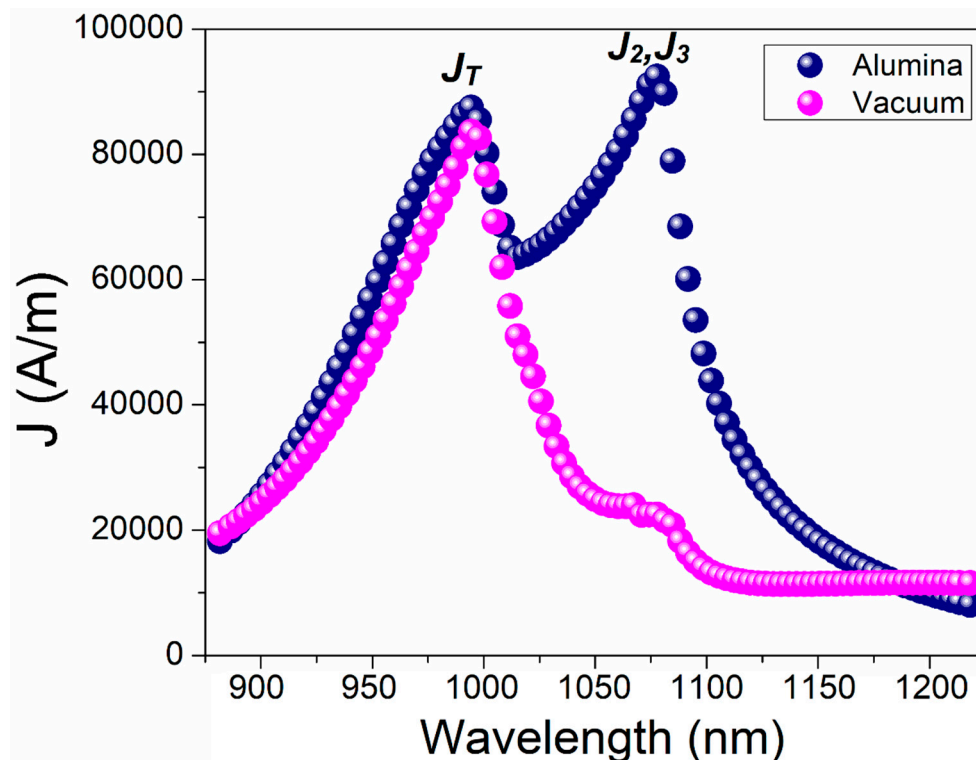
Figure 5. The characteristic surface current density map as a function of incidence, calculated for vacuum and alumina-filled gap regimes, showing the contribution of the super-toroidal mode in the formation of a second current density extreme.

4. Numerical Analysis

Here by using 3D simulation analysis based on the finite-difference time-domain (FDTD, Lumerical) approach, we demonstrated the formation of a high-order super-toroidal feature in the proposed nanostructure. In our simulations, to obtain the spectral response of the tailored nanostructures, the following parameters were utilized. The spatial gridding cell sizes were set to 0.5 nm in all axes, with 128 perfectly matched layers (PMLs) as absorptive boundaries. To satisfy the Courant stability, we set the simulation time step to 0.01 fs, and the NIR light source was a plane wave with a simulation duration of 400 fs. The dielectric functions for the Al meta-atoms were modeled by using the modified Drude response [27]:

$$\varepsilon_{Al} = \varepsilon_\infty - \frac{\omega_p^2}{\omega^2 + i\omega\Gamma} \tag{12}$$

in which ω_p is the bulk plasmon frequency, Γ is the damping constant (set to 1 eV), and ε_∞ is the high-frequency response (set to 3). As for the material selection of the resonator, Al was chosen because of its low-cost and abundance. The current density profile was calculated using the displacement current simulation module based on implementing the effective permittivity of the system ($\vec{D} = \varepsilon_{eff}\vec{E}$). Consequently, the current density was solved in FDTD simulations via the following equation: $\vec{J} = -i\omega(\varepsilon_{ff} - \varepsilon_0)\vec{E}$. For analytical computations, we developed an implementation of FDTD, known as bodies of revolution [28], to define the toroidal currents to the program. This approach utilizes the azimuthal symmetry, which reduces the complexity of the problem to a 2D simulation. By solving Maxwell's ρ-z plane with the actual 3D displacement current, we precisely defined the spectral properties of the unit cell by rotating the 2D solution around the *z*-axis.

5. Conclusions

In this work, we have revealed the physical significance of the contributions to the multi-loop charge–current configurations by studying the physics behind it. By using both theory and simulation analyses, we have recognized the excitation of complex multi-loop arrangements by providing a general approach for the observation of these moments in planar systems. To this end, we have reported the first numerical observation of a super-toroidal feature in plasmonic metamaterials across the NIR. Our observations of multi-loop currents (super-toroidal mode) in planar meta-atoms were accomplished by applying perturbations in the capacitive openings between the proximal nanopixels. Such a practical and fundamental approach allowed us to enhance the surface current density via the excitation of high-order multi-loop toroidal features. We believe that the methodology provided here can be effectively employed for development of high-order toroidal currents with ultra-high sensitivity to the surrounding perturbations such as precise plasmonic immunosensors and nanophotonic devices.

Supplementary Materials: The following are available online at http://www.mdpi.com/2304-6732/6/2/43/s1, Figure S1: Theoretically computed transmission spectrum, Figure S2: Magnetic field intensity.

Author Contributions: Conceptualization, B.G. and A.A.; Formal analysis, B.G. and A.A.; Writing, review and editing, B.G. and A.A.; Project administration, B.G. and A.A.

Conflicts of Interest: The authors declare no conflict of interest.

References

1.　Schwartz, M. *Principles of Electrodynamics*; McGraw-Hill: New York, NY, USA, 1972.
2.　Nanz, S. *Toroidal Multipole Moments in Classical Electrodynamics*; Springer Spektrum: Karlsruhe, Germany, 2016.
3.　Lesch, H.; Crusius, A.; Schlickeiser, R.; Wielebinski, R. Ring currents and poloidal magnetic fields in nuclear regions of galaxies. *Astron. Astrophys.* **1989**, *217*, 99–107.
4.　Papasimakis, N.; Fedotov, V.A.; Savinov, V.; Raybould, T.A.; Zheludev, N.I. Electromagnetic toroidal excitations in matter and free space. *Nat. Mater.* **2016**, *15*, 263–271. [CrossRef]
5.　Kaelberer, T.; Fedotov, V.A.; Papasimakis, N.; Tsai, D.P.; Zheludev, N.I. Toroidal dipolar response in a metamaterial. *Science* **2010**, *330*, 1510–1512. [CrossRef] [PubMed]
6.　Papasimakis, N.; Fedotov, V.A.; Marinov, K.; Zheludev, N.I. Gyrotropy of a metamolecule: Wire on a torus. *Phys. Rev. Lett.* **2009**, *103*, 093901. [CrossRef] [PubMed]
7.　Ahmadivand, A.; Gerislioglu, B.; Manickam, P.; Kaushik, A.; Bhansali, S.; Nair, M.; Pala, N. Rapid detection of infectious envelope proteins by magnetoplasmonic toroidal Metasensors. *ACS Sens.* **2017**, *2*, 1359–1368. [CrossRef] [PubMed]
8.　Gupta, M.; Srivastava, Y.K.; Singh, R. A Toroidal Metamaterial Switch. *Adv. Mater.* **2018**, *30*, 1704845. [CrossRef]
9.　Ahmadivand, A.; Gerislioglu, B.; Tomitaka, A.; Manickam, P.; Kaushik, A.; Bhansali, S.; Nair, M.; Pala, N. Extreme sensitive metasensor for targeted biomarkers identification using colloidal nanoparticles-integrated plasmonic unit cells. *Biomed. Opt. Express* **2018**, *9*, 373–386. [CrossRef]
10.　Ahmadivand, A.; Gerislioglu, B.; Pala, N. Large-modulation-depth polarization-sensitive plasmonic toroidal terahertz metamaterial. *IEEE Photonics Technol. Lett.* **2017**, *29*, 1860–1863. [CrossRef]
11.　Ahmadivand, A.; Gerislioglu, B. Toroidal plasmonic meta-biosensors: Benchmarking against classical plasmonic biosensors and transducers. *arXiv* **2018**, arXiv:1809.
12.　Ahmadivand, A.; Gerislioglu, B. Directional toroidal dipoles driven by oblique poloidal and loop currents flows in plasmonic meta-atoms. *J. Phys. Chem. C* **2018**, *122*, 24304–24308. [CrossRef]
13.　Ahmadivand, A.; Gerislioglu, B.; Pala, N. Active control over the interplay between the dark and hidden sides of plasmonics using metallodielectric Au-$Ge_2Sb_2Te_5$ unit cells. *J. Phys. Chem. C* **2017**, *121*, 19966–19974. [CrossRef]
14.　Gerislioglu, B.; Ahmadivand, A.; Pala, N. Tunable plasmonic toroidal terahertz metamodulator. *Phys. Rev. B* **2018**, *97*, 161405. [CrossRef]

15. Savinov, V.; Fedotov, V.A.; Zheludev, N.I. Toroidal dipolar excitation and macroscopic electromagnetic properties of metamaterials. *Phys. Rev. B* **2014**, *89*, 205112. [CrossRef]

16. Sayanskiy, A.; Danaeifar, M.; Kapitanova, P.; Miroshnichenko, A.E. All-dielectric metalattice with enhanced toroidal dipole response. *Adv. Opt. Mater.* **2018**, *6*, 1800302. [CrossRef]

17. Xu, L.; Rahmani, M.; Kamali, K.Z.; Lamprianidis, A.; Ghirardini, L.; Sautter, J.; Camacho-Morales, R.; Chen, H.; Parry, M.; Staude, I.; et al. Boosting third-harmonic generation by a mirror-enhanced anapole resonator. *Light Sci. Appl.* **2018**, *7*, 44. [CrossRef] [PubMed]

18. Xu, S.; Sayanskiy, A.; Kupriianov, A.S.; Tuz, V.R.; Kapitanova, P.; Sun, H.-B.; Han, W.; Kivshar, Y.S. Experimental observation of toroidal dipole modes in all-dielectric metasurfaces. *Adv. Opt. Mater.* **2019**, *7*, 1801166. [CrossRef]

19. Afanasiev, G.N.; Nelhiebel, M.; Stepanovsky, Y.P. The interaction of magnetizations with an external electromagnetic field and a time-dependent magnetic Aharonov-Bohm effect. *Phys. Scr.* **1996**, *54*, 417–427. [CrossRef]

20. Afanasiev, G.N.; Stepanovsky, Y.P. The electromagnetic field of elementary time-dependent toroidal sources. *J. Phys. A Math. Gen.* **1995**, *28*, 4565–4580. [CrossRef]

21. Afanasiev, G.N. Simplest sources of electromagnetic fields as a tool for testing the reciprocity-like theorems. *J. Phys. D Appl. Phys.* **2001**, *34*, 539–559. [CrossRef]

22. Nemkov, N.A.; Basharin, A.A.; Fedotov, V.A. Electromagnetic sources beyond common multipoles. *Phys. Rev. A* **2018**, *98*, 023858. [CrossRef]

23. Dubovik, V.; Tugushev, V. Toroid moments in electrodynamics and solid-state physics. *Phys. Rep.* **1990**, *187*, 145. [CrossRef]

24. Kong, J.A. *Electromagnetic Wave Theory*; John Wiley: Hoboken, NJ, USA, 1990.

25. Boardman, A.D.; Marinov, K.; Zheludev, N.; Fedotov, V.A. Nonradiating toroidal structures. *Spie Metamaterials* **2005**, *5955*, 595504.

26. Jackson, J.D. *Classical Electrodynamics*; Wiley: Hoboken, NJ, USA, 1999.

27. Palik, E.D. *Handbook of Optical Constants of Solids*; Academic Press: Orlando, FL, USA, 1985.

28. Taflove, A.; Hagness, S. *Computational Electrodynamics: The Finite-Difference Time-Domain Method*; Artech House: Norwood, MA, USA, 2000.